Isotopic composition for source identification of mercury in atmospheric fine particles

Qiang Huang[1], Jiubin Chen[1,*], Weilin Huang[2], Pingqing Fu[3], Benjamin Guinot[4], Xinbin Feng[1], Lihai Shang[1], Zhuhong Wang[1], Zhongwei Wang[1], Shengliu Yuan[1], Hongming Cai[1], Lianfang Wei[3] and Ben Yu[1]

[1]SKLEG, Institute of Geochemistry, Chinese Academy of Sciences, Guiyang 550081, China

[2]Department of Environmental Sciences, Rutgers, The State University of New Jersey, New Brunswick, NJ 08901, USA

[3]LAPC, Institute of Atmospheric Physics, Chinese Academy of Sciences, Beijing 100029, China

[4]Laboratoire d'Aérologie UMR5560 CNRS-Université Toulouse 3, Toulouse, France

* Corresponding author.

E-mail: chenjiubin@vip.gyig.ac.cn   Tel.: +86 851 85892269.

Abstract. The usefulness of mercury (Hg) isotopes for tracing the sources and pathways of Hg (and its vectors) in atmospheric fine particles ($PM_{2.5}$) is uncertain. Here, we measured Hg isotopic compositions in 30 potential source materials and 23 $PM_{2.5}$ samples collected in four seasons from the megacity Beijing (China), and combined the seasonal variation of both mass-dependent fractionation (represented by the ratio $^{202}Hg/^{198}Hg$, $\delta^{202}Hg$) and mass-independent fractionation of isotopes with odd and even mass numbers (represented by $\Delta^{199}Hg$ and $\Delta^{200}Hg$, respectively) with geochemical parameters and meteorological data to identify the sources of $PM_{2.5}$-Hg and possible atmospheric particulate Hg transformation. All $PM_{2.5}$ samples were highly enriched in Hg and other heavy metals, and displayed wide ranges of both $\delta^{202}Hg$ (−2.18 ‰ to 0.51 ‰) and $\Delta^{199}Hg$ (−0.53 ‰ to 0.57 ‰), and small positive $\Delta^{200}Hg$ (0.02 ‰ to 0.17 ‰). The results indicated that the seasonal variation of Hg isotopic composition (and elemental concentrations) was likely derived from variable contributions from anthropogenic sources, with continuous input due to industrial activities (e.g. smelting, cement production and coal combustion) in all seasons, whereas coal combustion dominated in winter and biomass burning mainly found in autumn. The more positive $\Delta^{199}Hg$ of $PM_{2.5}$-Hg in spring and early summer was likely derived from long-range transported Hg that had undergone extensive photochemical reduction. The study demonstrated that Hg isotopes may be potentially used for tracing the sources of particulate Hg and its vectors in the atmosphere.

Keywords: Mercury isotopic composition; Nonferrous metal smelting; Biomass burning; Long-range transport; Elemental carbon; Trace elements

1 Introduction

Mercury (Hg) is a globally distributed hazardous metal and is well known for its long-range transport, environmental persistence and toxicity (Kim et al., 2009; Selin, 2009; Schleicher et al., 2015). Hg is emitted to the atmosphere through natural and anthropogenic processes or reemission of previously deposited legacy Hg. It has three operationally defined forms: gaseous elemental Hg (GEM), reactive gaseous Hg (RGM) and particle-bound Hg (PBM) (Selin, 2009). In general, GEM (> 90 % of the total Hg in atmosphere) is fairly stable and can be transported globally, whereas RGM is rapidly deposited from the atmosphere in wet and dry deposition, and PBM is assumed to be transported more regionally (Selin, 2009; Fu et al., 2012). Recent measurements of PBM in several rural/urban areas have shown that Hg associated with particulate matter (PM) of size < 2.5 μm ($PM_{2.5}$-Hg) has typical concentrations <100 pg m^{-3} in background atmospheric environments (Liu et al., 2007; Fu et al., 2008; Kim et al., 2012), but exceeds 300 pg m^{-3} in contaminated regions (Xiu et al., 2009; Zhu et al., 2014). $PM_{2.5}$-Hg is of particular concern because, once inhaled, both Hg and its vectors might have adverse effects on human beings.

Mercury has seven stable isotopes (^{196}Hg, ^{198}Hg, ^{199}Hg, ^{200}Hg, ^{201}Hg, ^{202}Hg and ^{204}Hg) and its isotopic ratios in the nature have attracted much interest in recent years (Yin et al., 2010; Hintelmann and Zheng, 2012; Blum et al., 2014; Cai and Chen, 2016). Previous studies have reported both mass-dependent fractionation (MDF, δ^{202}Hg) and mass-independent fractionation (MIF, primarily observation of odd atomic weighed Hg isotopes, Δ^{199}Hg and Δ^{201}Hg) of Hg isotopes in environments (Hintelmann and Lu, 2003; Jackson et al., 2004; Bergquist and Blum, 2007; Jackson et al., 2008; Gratz et al., 2010; Chen et al., 2012; Sherman et al., 2012). The nuclear volume effect (NVE) (Schauble, 2007) and magnetic isotope effect (MIE) (Buchachenko, 2009) are thought to be the main causes for odd-MIF (Bergquist and Blum, 2007; Gratz et al.,

2010; Wiederhold et al., 2010; Sonke, 2011; Chen et al., 2012; Ghosh et al., 2013; Eiler et al.,

60   2014). Theoretical and experimental data suggested a $\Delta^{199}Hg/\Delta^{201}Hg$ ratio about 1.6 for NVE

(Zheng and Hintelmann, 2009, 2010b), and a $\Delta^{199}Hg/\Delta^{201}Hg$ ratio mostly between 1.0 and 1.3 for

MIE as a result of photolytic reductions under aquatic (and atmospheric) conditions (Zheng and

Hintelmann, 2009; Malinovsky et al., 2010; Wiederhold et al., 2010; Zheng and Hintelmann,

2010a; Sonke, 2011; Ghosh et al., 2013; Eiler et al., 2014). Over the past decade, studies

65   indicated that Hg isotope ratios are useful for differentiating Hg sources in terrestrial samples,

such as sediments (Jackson et al., 2004; Feng et al., 2010; Ma et al., 2013), soils (Biswas et al.,

2008; Zhang et al., 2013a) and biota (Sherman et al., 2013; Yin et al., 2013; Jackson, 2015), and

for distinguishing potential biogeochemical processes that Hg had undergone (Jackson et al.,

2013; Sherman et al., 2013; Yin et al., 2013; Masbou et al., 2015). Up to now, several studies

70   reported Hg isotopic compositions in atmospheric samples (Zambardi et al., 2009; Gratz et al.,

2010; Chen et al., 2012; Sherman et al., 2012; Demers et al., 2013; Rolison et al., 2013; Fu et al.,

2014; Demers et al., 2015a; Sherman et al., 2015; Yuan et al., 2015; Das et al., 2016; Enrico et al.,

2016; Fu et al., 2016). These studies reported large variations of $\Delta^{199}Hg$ and $\delta^{202}Hg$ values for

GEM (ranged from −0.41 ‰ to 0.06 ‰ for $\Delta^{199}Hg$, and from −3.88 ‰ to 1.43 ‰ for $\delta^{202}Hg$,

75   respectively) (Zambardi et al., 2009; Gratz et al., 2010; Sherman et al., 2010; Rolison et al., 2013;

Yin et al., 2013; Demers et al., 2015b; Das et al., 2016; Enrico et al., 2016; Fu et al., 2016) and

for Hg in precipitation (from 0.04 ‰ to 1.16 ‰ for $\Delta^{199}Hg$, and from −4.37 ‰ to 1.48 ‰ for

$\delta^{202}Hg$, respectively) (Gratz et al., 2010; Chen et al., 2012; Sherman et al., 2012; Demers et al.,

2013; Sherman et al., 2015; Wang et al., 2015b; Yuan et al., 2015). In addition, recent studies

80   have found MIF of even Hg isotopes (even-MIF, $\Delta^{200}Hg$) in natural samples mainly related to the

atmosphere, rendering Hg a unique heavy metal having "three-dimensional" isotope systems

(Chen et al., 2012).

While Hg isotopes in both GEM and RGM have drawn much attention, those of PBM are comparably less studied in the literature. Indeed, only several prior studies have focused on Hg isotopes in PBM. Rolison et al. (2013) reported, for the first time, δ^{202}Hg (of −1.61 ‰ to −0.12 ‰) and Δ^{199}Hg values (of 0.36 ‰ to 1.36 ‰) for PBM from the Grand Bay area in USA, and the ratios of Δ^{199}Hg/Δ^{201}Hg close to 1 that was thought to be derived from in-aerosol photo-reduction. Huang et al. (2015) measured Hg isotope ratios for two $PM_{2.5}$ samples taken from Guiyang of China, with δ^{202}Hg of −1.71 ‰ and −1.13 ‰ and Δ^{199}Hg of 0.21 ‰ and 0.16 ‰, respectively. Das et al. (2016) measured Hg isotopic compositions of PBM in PM_{10} from Kolkata, Eastern India and found negative MDF and varied values of Δ^{199}Hg between −0.31 ‰ to 0.33 ‰. These studies showed that the Hg isotope approach could be developed for tracking the sources and pathways of Hg species in the atmosphere.

China is one of the largest Hg emission countries in the world (Fu et al., 2012; Zhang et al., 2015), with a total estimated anthropogenic Hg emission of approximately 356 t in 2000 and 538 t in 2010 (Zhang et al., 2015). Coal combustion, nonferrous metal smelting, and cement production are the dominant Hg emission sources in China (collectively accounting for approximately over 80 % of the total Hg emission) (Zhang et al., 2015). Haze particles, especially $PM_{2.5}$ that are actually among the most serious atmospheric pollutants in urban areas of China (Huang et al., 2014), are one of the important carriers of Hg (Lin et al., 2015b; Schleicher et al., 2015). If $PM_{2.5}$ is emitted from the same source as Hg (Huang et al., 2014; Lin et al., 2015b; Schleicher et al., 2015; Zhang et al., 2015), quantifying Hg isotopes may provide direct evidence for the sources of both Hg and $PM_{2.5}$ as well as the insight to the geochemical processes that they may have undergone.

In this study, we attempted to identify the sources of $PM_{2.5}$-Hg in Beijing, the capital of China, using Hg isotopic composition coupled with meteorological and other geochemical parameters.

We selected Beijing as the study site because like many other Chinese megacities, Beijing has suffered severe $PM_{2.5}$ pollution (Huang et al., 2014; Gao et al., 2015) and is considered as the most PBM polluted area in China (Schleicher et al., 2015). In the past decade, only a few prior studies quantified the Hg concentrations in $PM_{2.5}$ samples collected from Beijing (Wang et al., 2006; Zhang et al., 2013b; Schleicher et al., 2015), while no research attempted to track its sources using the Hg isotope approach. The specific objectives of this study were 1) to characterize the seasonal variation of Hg isotope compositions in $PM_{2.5}$ of Beijing and 2) to test the effectiveness of the Hg isotope technique for tracking the sources of the $PM_{2.5}$-Hg.

2 Materials and methods

2.1 Field site and sampling method

Beijing (39.92 °N and 116.46 °E) has a population of over 21 million. It is located in a temperate warm zone with typical continental monsoon climate. The northwestern part of the Great Beijing Metropolitan is mountainous, while the southeastern part is flat. It has an average annual temperature of about 11.6 ℃, with the mean value of 24 ℃ in summer and −2 ℃ in winter. In the summer, wind blows mainly from southeast under influence of hot and humid East Asian monsoon, whereas the cold and dry monsoon blows from Siberia and Mongolia in the winter. The winter heating season in Beijing normally starts on 15 Nov and ends on 15 Mar.

$PM_{2.5}$ was sampled from Sep 2013 to Jul 2014 using a high volume $PM_{2.5}$ sampler placed on a building roof (approximately 8 m above the ground) of the Institute of Atmospheric Physics, Chinese Academy of Sciences, which is located between the north 3rd and 4th ring of Beijing. The meteorological model showed that the arriving air masses were transported mainly by two directions, with the northwest winds dominated in winter and the southern winds mainly in summer. The sampling information is detailed in Supporting Information (see Table S1). The $PM_{2.5}$ samples were collected using a Tisch Environmental $PM_{2.5}$ high volume air sampler, which

collects particles at a flow rate of 1.0 m^3 min^{-1} through a $PM_{2.5}$ size selective inlet. As the particles travel through the size selective inlet the larger particles are trapped inside of the inlet while the smaller-size ($PM_{2.5}$) particles continue to travel through the $PM_{2.5}$ inlet and are collected on a pre-combusted (450 ℃ for 6 hrs) quartz fiber filter (Pallflex 2500 QAT-UP, 20 cm × 25 cm, Pallflex Product Co., USA). The mass of $PM_{2.5}$ on each filter was measured using a gravimetric method by the mass difference before and after sampling. The filters were conditioned in a chamber with a relative humidity of about 48% and a temperature of 20±2 ℃ for about 24 h before and after sampling. A field blank was also collected during sampling and the value (< 0.2 ng of Hg, $n = 6$) was negligible (< 2 %) compared to the total Hg mass contained in the $PM_{2.5}$ samples. After sampling, each filter was recovered, wrapped with a pre-combusted (to eliminate Hg) aluminum film, and packed in a sealed plastic bag. The filters were brought back to the laboratory and stored at −20 ℃ prior to analysis.

In order to better assign sources of Hg, we collected and measured 30 solid samples of different materials that may be potential Hg (and $PM_{2.5}$) sources and that may contribute to $PM_{2.5}$-Hg in Beijing. They included: (i) eight samples (including feed coal powder, bottom ash, desulfurization gypsum and fly ash) from two coal-fired power plants (from Hubei and Mongolia provinces); (ii) six samples from a Pb-Zn smelting plant (including blast furnace dust, dust of blast furnace slag, sintering dust, coke, return powder and agglomerate); (iii) ten samples from a cement plant (including coal powder, raw meal, sandstone, clay, limestone, steel slag, sulfuric acid residue, desulfurization gypsum and cement clinker), six of which were published previously (Wang et al., 2015b); (iv) four topsoil samples (surface horizon: organics mixed with mineral matter, these samples are not natural soil on typical soil profiles) from the center city of Beijing (Olympic Park, Beihai Park, the Winter Palace and Renmin University of China (RUC)), two dust samples from RUC (one building roof dust and one road dust); (v) one total suspended

155 particle (TSP, the sampling of TSP was carried out using a made in house low volume (about 1.8

$m^3 h^{-1}$) air sampler equipped with a TSP inlet, and a pre-cleaned mixed fiber filter (47 mm) was

used for the TSP low-volume inlets) sample from atmosphere of rural area of Yanqing district,

northwest of Beijing; and (vi) two urban road dust, two suburban road dust and one suburban

topsoil samples from Shijiazhuang city southwest from Beijing. Though the automobile exhausts

160 might also be a contributing source of $PM_{2.5}$-Hg, we were not able to measure its Hg isotope

ratios due to its exceedingly low Hg concentration (Won et al., 2007).

2.2 Materials and reagents

Materials and reagents used in this study were similar to those described in previous study

(Huang et al., 2015). A 0.2 M BrCl solution was prepared by mixing the distilled concentrated

165 HCl with pre-heated (250 ℃, 12 hrs) KBr and $KBrO_3$ powders. Two $SnCl_2$ solutions of 20 and

3 % (wt) were prepared by dissolving the solid in 1 M HCl and were used for on-line reduction of

Hg for concentration and isotope measurements, respectively. A 20 % (wt) $NH_2OH•HCl$ solution

was used for BrCl neutralization.

Two international Hg standards NIST SRM 3133 and UM-Almaden were used as the

170 reference materials for Hg isotope analysis. NIST SRM 997 Thallium (20 ng mL^{-1} Tl in 3 %

HNO_3) was employed for mass bias correction (Chen et al., 2010; Huang et al., 2015). Two other

reference materials, the solution Fluka 28941 Hg (TraceCERT®, Sigma-Aldrich) and the soil

GBW07405 (National Center for Standard Materials, Beijing, China) were used as in-house

isotope standards, and were regularly measured for quality control of Hg concentration and

175 isotope measurements. It was noteworthy that Fluka 28941 Hg is a standard different from ETH

Fluka Hg (Jiskra et al., 2012; Smith et al., 2015).

2.3 Isotopic Composition Analysis.

Mercury bound on $PM_{2.5}$ and solid source materials was released via a dual-stage combustion protocol and it was captured in a 5-mL 40% acid mixture (2:4:9 volumetric ratio of 10 M HCl, 15 M HNO_3 and Milli-Q water) (Huang et al., 2015). Detailed procedure is available in Huang et al. (2015). In brief, the filter samples were rolled into a cylinder and placed in a furnace quartz tube (25 mm OD, 22 mm ID, 1.0 m length), which was located in two combustion tube furnaces (BTF-1200C-S, Anhui BEQ Equipment Technology Ltd., China). The solid source samples were powdered and weighted into a sample quartz tube (20 mm OD, 18 mm ID, 10 cm length), which was capped with quartz wool (pre-cleaned at 500 ℃) at both ends to prevent particle emission. The sample tube was then placed into the large quartz tube of the furnace. The samples were combusted through a temperature-programmed routine in the dual-stage combustion and acid solution trapping system. An aliquot (50 μL) of 0.2 M BrCl was added to the above trapping solution to stabilize the Hg^{2+}. The trapping solution for each sample was diluted to a final acid concentration of about 20 % and was stored at 4 ℃ for the subsequent Hg concentration and isotope measurement. The accuracy and precision of the dual-stage combustion protocol were evaluated by the analysis of the certified reference material GBW07405 using the same digestion method. The detectable Hg in the procedural blank (< 0.2 ng, $n = 12$) of this dual-stage combustion method was negligible compared to the amount of total Hg (> 5 ng) in both $PM_{2.5}$ samples and procedural standards.

Mercury isotope analyses were performed on the MC-ICP-MS (Nu Instruments Ltd., UK) at the State Key Laboratory of Environmental Geochemistry, Institute of Geochemistry, China. The details of the analytical procedures and the instrumental settings were given in previous studies (Huang et al., 2015; Lin et al., 2015a; Wang et al., 2015b; Yuan et al., 2015). In brief, a home-made cold-vapor generation system was coupled with an Aridus II Desolvating Nebulizer for respective Hg and Tl introductions. The Faraday cups were positioned to simultaneously collect

five Hg isotopes and two Tl isotopes including ^{205}Tl (H3), ^{203}Tl (H1), ^{202}Hg (Ax), ^{201}Hg (L1), ^{200}Hg (L2), ^{199}Hg (L3), and ^{198}Hg (L4). The instrumental mass bias was double corrected by both internal standard NIST SRM 997 Tl and by sample-standard bracketing (SSB) using international standards NIST SRM 3133 Hg. The MDF of isotopes is represented by delta (δ) notation in units of permil (‰) and defined as the following equation (Blum and Bergquist, 2007):

$$\delta^{x}\text{Hg (‰)} = [(^{x}\text{Hg}/^{198}\text{Hg})_{sample}/(^{x}\text{Hg}/^{198}\text{Hg})_{NIST3133} - 1] \times 1000 \quad (1)$$

where x = 199, 200, 201, and 202. MIF is reported as the deviation of a measured delta value from the theoretically predicted value due to kinetic MDF according to the equation:

$$\Delta^{x}\text{Hg (‰)} = \delta^{x}\text{Hg} - \beta \times \delta^{202}\text{Hg} \quad (2)$$

where the mass-dependent scaling factor β is of about 0.252 0.5024 and 0.752 for ^{199}Hg, ^{200}Hg and ^{201}Hg, respectively (Blum and Bergquist, 2007).

The Fluka 28941 Hg standard was carefully calibrated against the NIST SRM 3133 Hg and the long-term measurements yielded an average value of -1.00 ± 0.13 ‰ (2SD, $n = 15$) for δ^{202}Hg, with a precision similar to that (0.10 ‰, $n = 114$) obtained for NIST SRM 3133 Hg. Our repeated measurements of UM-Almaden and GBW07405 had average δ^{202}Hg, Δ^{199}Hg and Δ^{201}Hg values of -0.60 ± 0.09 ‰, -0.01 ± 0.06 ‰ and -0.03 ± 0.06 ‰ (2SD, $n = 18$) and of -1.77 ± 0.14 ‰, -0.29 ± 0.04 ‰ and -0.32 ± 0.06 ‰ (2SD, $n = 6$), respectively, consistent with the data published in previous studies (Blum and Bergquist, 2007; Zheng et al., 2007; Smith et al., 2008; Carignan et al., 2009; Zambardi et al., 2009; Chen et al., 2010; Sherman et al., 2010; Wiederhold et al., 2010; Huang et al., 2015). In this study, the 2SD uncertainties (0.14 ‰, 0.04 ‰ and 0.06 ‰ for δ^{202}Hg, Δ^{199}Hg and Δ^{201}Hg) obtained for the soil reference GBW07405 were considered as the typical external uncertainties for some PM$_{2.5}$ samples that were measured only once due to their limited mass. Otherwise, the uncertainties were calculated based on the multiple measurements (Tables S1 and S2).

2.4 Concentration measurements

A small fraction of each trapping solution (20 % acid mixture) was used to measure the Hg concentration on CVAFS (Tekran 2500, Tekran® Instruments Corporation, CA), with a precision better than 10 %. The recoveries of Hg for the standard GBW07405 and 30 solid samples were in the acceptable range of 95 to 105 %; but no recovery of Hg for the $PM_{2.5}$ samples was determined due to limited availability of the samples. A 0.5 cm^2 punch from each filter samples was analyzed for organic and elemental carbon (OC/EC) with a Desert Research Institute (DRI) Model 2001 Thermal/Optical Carbon Analyzer (Atmoslytic Inc., Calabasas, CA, USA) following the Interagency Monitoring of Protected Visual Environments (IMPROVE) thermal evolution protocol (Wang et al., 2005). The calculated uncertainties were ± 10 % for the measured OC and EC data. The concentrations of other elements (e.g. Al, Cd, Co, Pb, Sb, Zn, K, Ca and Mg) were also measured for 14 of the $PM_{2.5}$ samples and 16 of the selected potential source materials using ICP-MS or ICP-AES after total acid (HNO_3-HF-$HClO_4$) digestion. A 1.5 cm^2 punch from each filter samples and about 0.05 g of solid material samples were dissolved completely with HNO_3-HF-$HClO_4$. Note that, due to limited mass of $PM_{2.5}$ samples, 9 $PM_{2.5}$ samples were exhausted after isotope analysis, and only 14 $PM_{2.5}$ samples were analyzed for the other elements. The soil standard GBW07405 was digested using the same protocol and the measured concentrations of trace elements (TEs, including Hg) were consistent with the certified values.

3 Results

3.1 General characteristics of $PM_{2.5}$

The contents of $PM_{2.5}$, OC and EC for the 23 samples are presented in Table S1. The volumetric contents of $PM_{2.5}$ ranged from 56 to 310 µg m^{-3} (average 120 ± 61 µg m^{-3}), and were higher in autumn than the three other seasons (Fig. 1). The $PM_{2.5}$ samples showed large variations of carbon concentrations, with OC ranged from 2.8 to 42 µg m^{-3} and EC from 1.2 to 9.2 µg m^{-3},

250　averaging of 12 ± 9.6 and 3.7 ± 2.3 µg m^{-3}, respectively. The OC and EC contents in autumn

(respective mean of 14 ± 11 and 4.9 ± 2.8 µg m^{-3}, $n = 6$) and winter (mean of 19 ± 13 and $5.1 \pm$

2.3 µg m^{-3}, $n = 6$) were approximately doubled compared to those in spring (mean of 7.7 ± 1.4

and 2.5 ± 0.7 µg m^{-3}, $n = 6$) and summer (mean of 5.9 ± 1.8 and 2.0 ± 0.5 µg m^{-3}, $n = 5$). Similar

seasonal variation was also reported in a previous study (Zhou et al., 2012). When converted to

255　the mass concentrations, the OC and EC contents were significantly ($p < 0.01$) higher in winter

(mean of 170 ± 49 and 50 ± 8 µg g^{-1}, $n = 6$) than in other seasons (mean of 71 ± 18 and 25 ± 7.3

µg g^{-1}, $n = 17$) (Table S1). Since EC contents were closely correlated to OC ($r^2 = 0.89$, $p < 0.001$),

we discuss only EC contents in the following as an indicator for the source of PM, because EC is

a significant pollutant of combustion source that is not readily modified by secondary processes

260　in the atmosphere.

FIGURE 1

3.2　Seasonal variation of mercury concentration and isotopic composition

PM$_{2.5}$-Hg volumetric concentrations and isotopic compositions are shown in Table S1. In general,

the PM$_{2.5}$-Hg concentrations ranged from 11 to 310 pg m^{-3}, with an average value of 90 ± 80 pg

265　m^{-3}. These values were comparable to those reported at a rural site of Beijing (98 ± 113 pg m^{-3})

(Zhang et al., 2013b), indoor PM$_{2.5}$ of Guangzhou (104 pg m^{-3}) (Huang et al., 2012) and several

southeastern coastal cities (141 ± 128 pg m^{-3}) of China (Xu et al., 2013), but they were lower

than those reported values for Guiyang (368 ± 676 pg m^{-3}) of China (Fu et al., 2011). From a

global perspective, our PM$_{2.5}$-Hg contents were much higher than those reported for urban areas

270　of other countries such as Seoul in South Korea (23.9 ± 19.6 pg m^{-3}) (Kim et al., 2009), Goteborg

in Sweden (12.5 ± 5.9 pg m^{-3}) (Li et al., 2008) and Detroit in USA (20.8 ± 30.0 pg m^{-3}) (Liu et

al., 2007). The averaged PM$_{2.5}$-Hg values showed an evident seasonal variation, with relatively

higher value in winter (140 ± 99 pg m^{-3}) and lower in summer (22 ± 8.2 pg m^{-3}) (see Figs. 1 and

2). Previous studies also reported similar variation for Hg loads in atmospheric particles in Beijing (Wang et al., 2006; Schleicher et al., 2015), for example, the highest value of $2,130 \pm 420$ pg m^{-3} was found in winter 2004 while lower values generally reported in summer (Wang et al., 2006; Schleicher et al., 2015).

<div align="center">FIGURE 2</div>

Seasonal variations were also observed for Hg isotopic compositions (see Figs. 1 and 2 and Table S1). The δ^{202}Hg values ranged from -2.18 ‰ to 0.51 ‰ (average -0.71 ± 0.58 ‰, 1SD, n = 23), with the lowest value of -2.18 ‰ found on 29 Jun 2014 (in summer) whereas the highest of 0.51 ‰ on 30 Sep 2013 (in autumn). Interestingly, all samples displayed a large Δ^{199}Hg variation from -0.53 ‰ to 0.57 ‰ (mean of 0.05 ± 0.29 ‰). Unlike δ^{202}Hg, the lowest Δ^{199}Hg value (-0.53 ‰) was found in autumn (on 30 Sep 2013), whereas the highest value (0.57 ‰) was observed in spring (23 Apr 2014). Positive even-MIF of Hg isotope was also determined in all PM$_{2.5}$-Hg, with Δ^{200}Hg ranging from 0.02 ‰ to 0.17 ‰, averaging 0.09 ± 0.04 ‰ (Table S1). Three previous studies reported negative δ^{202}Hg (from -3.48 ‰ to -0.12 ‰) but significantly positive Δ^{199}Hg (from -0.31 ‰ to 1.36 ‰) for atmospheric particles (Rolison et al., 2013; Huang et al., 2015; Das et al., 2016).

3.3 Mercury content and isotope ratios in potential source materials

As showed in Table S2, the Hg concentrations of the potential source materials ranged widely from 0.35 to 7,747 ng g^{-1}, with an exceptionally high value of 10,800 ng g^{-1} for the sintering dust collected by the electrostatic precipitator in a smelting plant. Though the topsoil and road dust samples generally displayed relatively lower Hg concentrations (e.g. 23 to 408 ng g^{-1}, Table S2), the topsoil collected from Beihai Park in 2nd ring of Beijing had an exceptionally high Hg content of 7,747 ng g^{-1}. To be noted, these data were comparable to the mass-based Hg concentrations (150 to 2,200 ng g^{-1} with a mean value of 720 ng g^{-1}) for the 23 PM$_{2.5}$ samples (Table S1).

The potential source materials also had a large variation of Hg isotope compositions (Figs. 2 and 3 and Table S2), with δ^{202}Hg ranging from -2.67 ‰ to 0.62 ‰ (average -0.98 ± 0.79 ‰, 1SD, $n = 30$), while Δ^{199}Hg ranged from -0.27 ‰ to 0.18 ‰ (mean -0.03 ± 0.11 ‰), and Δ^{200}Hg values from -0.04 ‰ to 0.11 ‰ (mean 0.02 ± 0.04 ‰).

FIGURE 3

4 Discussion

Previous studies demonstrated that coal combustion, cement plant and non-ferrous metal smelting were main sources of Hg in the atmosphere (Streets et al., 2005; Zhang et al., 2015), contributing about 47, 18.5 and 17.5 % of total anthropogenically-emitted Hg in China, respectively (Zhang et al., 2015). In particular, special events such as large-scale biomass burning in autumn and excessive coal combustion in the winter heating season might also have overprinted the concentration of PM$_{2.5}$-Hg and its isotope composition. In addition to the possible direct emission from the above anthropogenic sources, atmospheric processes may have impacted the PM$_{2.5}$-Hg isotopic composition, particularly during the long-range transportation of PM$_{2.5}$-Hg (thus long residence time of about a few days to weeks) in the atmosphere (Lin et al., 2007). These potential sources and possible process effects are discussed in the following sections.

4.1 Evidence for strong anthropogenic contribution

Anthropogenic emission as the main PM$_{2.5}$-Hg contributing sources is evidenced by the enrichment factor (EF) of Hg (and other metals), which was a commonly-used geochemical indicator for quantifying the enrichment/depletion of a targeted element in environmental samples (Gao et al., 2002; Song et al., 2012; Chen et al., 2014; Mbengue et al., 2014; Lin et al., 2015b). The EF of a given element was calculated using a double normalization (to the less reactive element Al here) and the upper continental crust (UCC) (Rudnick and Gao, 2003) was chosen as the reference (see detailed in Supporting Information). Al is well adapted to this

normalization as it has usually no anthropogenic origin and is not readily modified by secondary processes in the atmosphere, and thus was widely used for enrichment calculation in atmospheric pollution studies (Gao et al., 2002; Waheed et al., 2011; Mbengue et al., 2014; Lin et al., 2015b).

325 The calculated results showed (Table S4) high EF(Hg) values for the 14 $PM_{2.5}$ samples, ranged from 66 to 424 with an average value of 228 ± 134 (1SD, $n = 14$), indicating that $PM_{2.5}$-Hg pollution was serious (characterized by significant Hg enrichment) in Beijing. As a TE, Hg concentration is generally low in natural terrestrial reservoirs (e.g. 50 ppb in UCC) (Rudnick and Gao, 2003). Similar to the UCC, the topsoil was also mainly composed of aluminosilicates with

330 relatively low Hg concentrations (Table S2). Thus, high EF(Hg) values probably implied a strong anthropogenic contribution to Hg in $PM_{2.5}$. This could be confirmed by very high EF(Hg) values (up to 226,000, Table S4) determined, for example, in three potential source materials collected from the smelting plant. The high EF(Hg)s also emphasize the importance of studying toxic metals such as Hg (and other heavy metals) in atmospheric particles while accessing the potential

335 threat of hazes on human health.

The strong anthropogenic contribution may be also supported by the relationships between Hg and other particulate components in $PM_{2.5}$. Figs. 4a and 4b showed very good correlations between $PM_{2.5}$-Hg concentration and the volumetric concentrations of $PM_{2.5}$ and EC, with correlation coefficient (r^2) of 0.40, and 0.80, respectively. It is well known that atmospheric

340 pollution due to the high concentrations of $PM_{2.5}$ and EC mainly results from anthropogenic emissions (Gao et al., 2015; Lin et al., 2015b). $PM_{2.5}$-Hg also displayed linear relationships with trace metals. Figs. 4c and 4d show the examples with Co and Zn (r^2 of 0.74 and 0.44, respectively, $p < 0.01$). High metal contents in atmospheric particles are generally related to human activities. For example, combustion and smelting release large amount of TEs into the atmosphere (Xu et

345 al., 2004; Nzihou and Stanmore, 2013). The fact that all $PM_{2.5}$ samples displayed very high EFs

for "anthropophile" elements (elements were generally enriched by human activities) (Chen et al., 2014) such as Cd, Cu, Pb, Sb, Se, Tl and Zn (ranging from 10 to 20,869, Table S4) clearly illustrated the anthropogenic contribution to these elements in $PM_{2.5}$. As a result, fine atmospheric particles in Beijing were strongly enriched in Hg and other TEs, which was likely caused by elevated anthropogenic activities.

FIGURE 4

4.2 Isotopic overprint of potential anthropogenic Hg sources

Hg isotopic signatures may further indicate that human activities contributed to a large proportion of $PM_{2.5}$-Hg. In this study, all samples displayed a large variation of δ^{202}Hg (from −2.18 ‰ to 0.51 ‰, Table S1), similar to those (from −2.67 ‰ to 0.62 ‰, Table S2) determined for the particulate materials from potential sources such as coal combustion (averaged −1.10 ± 1.20 ‰, 1SD, n = 8), smelting (−0.87 ± 0.82 ‰, 1SD, n = 6) and cement plants (−1.42 ± 0.36 ‰, 1SD, n = 10), as demonstrated in Figs. 2 and 3. This similarity might indicate the emission of these anthropogenic sources as the possible contributing sources of $PM_{2.5}$-Hg. Though the anthropogenic samples collected in this study could not cover the whole spectrum of anthropogenic contributions, previous studies reported similar δ^{202}Hg range (from −3.48 ‰ to 0.77 ‰) for potential source materials worldwide (Biswas et al., 2008; Estrade et al., 2011; Sun et al., 2013; Sun et al., 2014; Yin et al., 2014; Wang et al., 2015b; Das et al., 2016). In fact, most $PM_{2.5}$ samples possessed Δ^{199}Hg similar to those determined in above-mentioned particulate materials (−0.27 ‰ to 0.04 ‰, Figs. 2 and 3) in this study, suggesting these anthropogenic emission as the major sources of $PM_{2.5}$-Hg.

Interestingly, Hg isotope compositions were correlated well with the elements such as Co, Ni and Sb (here mass ratio of the element/Al was used to cancel out the dilution effect by major mineral phase), as shown in Figs. 5a and 5b for the example of Co. These correlations might

370   indicate that Hg and some other metals had common provenance, likely from anthropogenic

combustion, as discussed above. A careful investigation of the correlations amongst metal

elements, along with Hg isotopic data, further indicated anthropogenic source category. The

principal component analysis (PCA) of Hg and other TEs (see Table S5) demonstrated likely that

four factors might control the variance of the entire data set over four seasons. In accordance with

375   the above discussion, these four factors were likely a mixture of coal combustion and nonferrous

metal smelting (characterized by high contents of Pb, Rb, Se, Zn, Tl, Cr and Cd), cement

production (enriched in Ca, Sr, Al and Mg), traffic emission and biomass burning, with their

contributions estimated to be about 39 %, 24 %, 23 %, and 7 % (Table S5).

FIGURE 5

380   As a result, the Hg isotopic compositions may potentially suggest that coal combustion,

smelting and cement plants were major sources of PM$_{2.5}$-Hg. The higher EF(Hg) values and the

detail investigation of elemental data supported this hypothesis. However, without careful

characterization of potential sources, we are unable to quantify the contribution from each source

at this stage. Noteworthily, Figs. 6a and 6b showed that δ^{202}Hg increased with EF(Hg) ($r^2 = 0.55$),

385   whereas Δ^{199}Hg decreased with EF(Hg) ($r^2 = 0.36$). These correlations may suggest that the large

isotope variation of PM$_{2.5}$-Hg might be mainly controlled by two endmembers with contrasting

δ^{202}Hg and Δ^{199}Hg. The end Δ^{199}Hg values of correlations, however, could not be explained by

the above defined anthropogenic sources, which generally had insignificant odd-MIF. The

contribution from additional sources or possible processes was thus needed to explain the

390   extreme Δ^{199}Hg values. Accordingly, the δ^{202}Hg and Δ^{199}Hg exhibited contrast relationships with

the EC/Al ratios (Figs. 5c and 5d). As relatively higher EC contents were generally derived from

coal combustion and biomass burning (Zhang et al., 2008; Saleh et al., 2014), these two non-

point emission sources might account for the Δ^{199}Hg end values.

FIGURE 6

4.3 Dominant contribution from coal combustion in winter

High EC content in winter PM$_{2.5}$ might result from additional coal combustion during the heating season, when coal was widely used in both suburban communities and rural individual families (Wang et al., 2006; Song et al., 2007; Schleicher et al., 2015). This additional coal burning could considerably increase Hg and EC emission, explaining the relatively higher PM$_{2.5}$-Hg (1340 ng g^{-1}, $p < 0.01$) and carbon contents (Table S1). In this study, both δ^{202}Hg (mean -0.71 ± 0.37 ‰) and Δ^{199}Hg (-0.08 ± 0.11 ‰, 1SD, $n = 6$) for winter PM$_{2.5}$ samples were consistent with those in coals (average δ^{202}Hg values of -0.73 ± 0.33 ‰ and Δ^{199}Hg of -0.02 ± 0.08 ‰, respectively) from northeastern China (Yin et al., 2014), possibly supporting the above conclusion. Beside EC contents, Zn/Al ratio may provide information for PM from industrial (e.g. metal smelting) emission sources. In Zn/Al vs. EC diagram (Fig. 7), all winter samples displayed a linear relationship ($r^2 = 0.94$) different from the samples of other seasons. Compared to the data of other seasons, the volumetric EC concentrations varied greatly in winter, whereas the Zn/Al ratio of the same season remained stable. This variation may be derived from the emission of coal burning that is characterized by high carbon content but relatively low Zn concentration (Nzihou and Stanmore, 2013; Saleh et al., 2014). This highlighted again the dominated contribution from coal combustion. The backward trajectory calculated by a Hybrid Single Particle Lagrangian Integrated Trajectory (HYSPLIT) model (Fig. S1) showed the dominant northwestern wind in winter. In this case, the fact that the transported air masses were derived from the background region (less populated and underdeveloped) could potentially explain both the lower volume-based concentrations of Hg, TEs (e.g. Zn) and EC (Fig. 7) and the higher mass-based contents of Hg, TEs (e.g. Zn) and EC (Table S1) in some winter samples. The dilution by this background air could also explain the comparable EC content in winter and autumn (Figs. 1 and 7).

FIGURE 7

4.4 Important biomass burning input in autumn

420   Biomass burning that often occurred in north China might be the cause of relatively higher EC volumetric concentrations in autumn PM$_{2.5}$. The HYSPLIT model (Fig. S2) showed that, unlike the winter PM$_{2.5}$, the samples collected in autumn were strongly impacted by northward wind. Biomass burning that occurred in the south of Beijing during autumn harvesting season could transport a large amount of EC (and Hg) to Beijing, adding a potential source to PM$_{2.5}$-Hg.

425   Though biomass burning is not an important source in an annual time scale (from PCA estimation), it may display major contribution in a shot time period in autumn. Previous studies showed that this source might account for 20 to 60 % of PM$_{2.5}$ in Beijing during peak days of biomass burning (Zheng et al., 2005a; Zheng et al., 2005b). Isotopically, PM$_{2.5}$ collected in the arriving air masses from south were characterized by significantly negative Δ^{199}Hg values (from

430   −0.54 ‰ to −0.29 ‰), whereas samples collected in the northwestern wind event exhibited Δ^{199}Hg values close to zero or slightly positive, indicating a negative Δ^{199}Hg signature in biomass burning emission Hg. Our newly obtained data on Hg isotopes from biomass burning showed negative Δ^{199}Hg (that will be published in the future), supporting our hypothesis. Moreover, prior studies have generally reported negative Δ^{199}Hg values for biological samples including foliage

435   (about −0.37 ‰), rice stem (about −0.37 ‰) and litter (about −0.44 ‰) (Demers et al., 2013; Yin et al., 2013; Jiskra et al., 2015), even down to −1.00 ‰ for some lichen (Carignan et al., 2009). The odd-MIF signature may be conserved during complete biomass burning as this process would not produce any mass-independent fractionation (Sun et al., 2014; Huang et al., 2015).

    Interestingly, the autumn PM$_{2.5}$ had a Zn/Al versus EC correlation (r^2 = 0.37) distinctly

440   different from the winter samples, and also from spring and summer samples (Fig. 7). This difference may imply another carbon-enriched contribution in autumn other than coal combustion.

In fact, the largely occurring biomass burning in the south (Hebei and Henan provinces) may lead to the EC content (volume-based) increasing in autumn air mass. Thus, the high EC air mass input from biomass burning could explain the different trend which defined by autumn $PM_{2.5}$, while the above-discussed contribution from industries (mainly smelting) could explain the higher Zn (at a given EC content) in summer samples. Though most samples with high EC could result from biomass burning, two autumn samples displayed relatively low EC could be caused by the dilution from northern background air mass (Fig. S2), as demonstrated by the HYSPLIT model.

4.5 Contribution from long-range transported $PM_{2.5}$-Hg

Besides the dominant contribution from local or regional emissions, long-range transported Hg might impact on $PM_{2.5}$-Hg in Beijing (Han et al., 2015; Wang et al., 2015a). As shown in Figs. 1 and 2 and Table S1, the six spring $PM_{2.5}$ samples and the one early summer sample had much high $\Delta^{199}Hg$ (from 0.14 ‰ to 0.57 ‰, mean of 0.39 ± 0.16 ‰, 1SD, $n = 7$) and $\Delta^{200}Hg$ values (from 0.08 ‰ to 0.12 ‰, mean of 0.10 ± 0.01 ‰, 1SD, $n = 7$). These high values could not be explained by the above defined anthropogenic contributors having generally negative or close to zero MIF (Figs. 2 and 3), yet another contribution or fractionation during atmospheric processing is needed to explain all data set. The long-range transported $PM_{2.5}$ may be such contributor in addition to the direct local or regional anthropogenic emission (Han et al., 2015; Wang et al., 2015a).

The HYSPLIT calculation showed that the arriving air masses of these samples generally came from a long distance (mainly from the North and Northwest, Figs. S3 and S4), suggesting a contribution of long-range transportation, given the residence time of $PM_{2.5}$-Hg (days to weeks) (Lin et al., 2007). Unfortunately, we were not able to collect and analyze the typical long-range transported Hg in this study. Previous studies have reported that long-range transported Hg might

exhibit relatively higher Δ^{199}Hg (up to 1.16 ‰) due to the extensive photolysis reaction (Chen et al., 2012; Wang et al., 2015b; Yuan et al., 2015). In fact, the samples with significantly positive Δ^{199}Hg were collected during a period (at least 3 days before sampling) with long daily sunshine (> 8.8 hrs) for Beijing and adjacent regions (Table S1). Such climate condition might be favorable for photo-reduction of atmospheric Hg^{2+}, which preferentially enriches odd isotopes in solution or aerosols. The fact that the background TSP sample from the Yanqing region had higher Δ^{199}Hg (0.18 ‰, Table S2) than PM$_{2.5}$ samples collected at the same time in Centre Beijing might suggest higher odd-MIF values for long-range transported Hg, since the local Hg emission is very limited in this rural area. Moreover, the higher Δ^{200}Hg values (from 0.08 ‰ to 0.12 ‰, Table S1) determined in these samples may also indicate the contribution of long-range transportation, since even-MIF was thought to be a conservative indicator of upper atmosphere chemistry (Chen et al., 2012; Cai and Chen, 2016). Since the locally emitted PM$_{2.5}$-Hg (having lower or close to zero Δ^{199}Hg and Δ^{200}Hg) mainly resided and accumulated in the atmosphere boundary layer (generally < 1000 m), and thus could be largely scavenged by precipitation (Yuan et al., 2015), the higher Δ^{199}Hg values (from 0.06 ‰ to 0.14 ‰, see Table S1) for PM$_{2.5}$ sampled after precipitation event supported the contribution of long-range transport to PM$_{2.5}$-Hg. Finally, as the background PM$_{2.5}$ with little input from anthropogenic activities are likely characterized by low contents of trace metals (such as Zn) and organic matter (Song et al., 2007; Zhou et al., 2012), the long-range transport contribution could also explain PM$_{2.5}$ samples with relatively low EC content and Zn/Al ratio in Fig. 7.

4.6 Possible process effects on transported PM$_{2.5}$-Hg

The atmospheric processes such as secondary aerosol production, adsorption (and desorption) and redox reactions may induce a redistribution of Hg among GEM, RGM and PBM, and simultaneously fractionate Hg isotopes in PM$_{2.5}$, possibly resulting in a difference of Hg isotopic

490   composition between $PM_{2.5}$ and source materials. Up to now, Hg isotopic fractionation is rarely

reported for Hg redistribution and secondary aerosol formation in the atmosphere. However, the

fact that the contents of secondary organic carbon (see detailed calculation in Supporting

Information) had no correlation ($r^2 < 0.09$, $p > 0.18$) with either $\delta^{202}Hg$ or $\Delta^{199}Hg$ may imply a

limited effect of such processes. Previous studies have showed limited adsorption of Hg^0 on

495   atmospheric particles (Seigneur et al., 1998). More importantly, according to the experiments

conducted under aqueous conditions, the adsorption/desorption and precipitation of Hg^{2+} may

only induce very small MIF of Hg isotopes (Jiskra et al., 2012; Smith et al., 2015), in contrast

with our observation. Therefore, the effect of adsorption or precipitation was probably limited on

MIF of isotopic composition of $PM_{2.5}$-Hg. In this study, all 23 $PM_{2.5}$ samples defined a straight

500   line in Fig. 2 with a $\Delta^{199}Hg/\Delta^{201}Hg$ slope of about 1.1, consistent with the results of Hg^{2+}

photoreduction experiment (Bergquist and Blum, 2007; Zheng and Hintelmann, 2009),

suggesting a possible effect of photochemical reduction during $PM_{2.5}$-Hg transport. Potentially,

the enrichment of odd isotopes in reactants (here particles) during these processes can explain the

positive $\Delta^{199}Hg$ in spring and summer samples. However, most samples collected in autumn and

505   winter displayed significant negative $\Delta^{199}Hg$ values (down to −0.54 ‰, Figs. 1, 2, 4 and 5, and

Table S1). Therefore, the photoreduction of divalent Hg species cannot explain the total variation

of Hg isotope ratios determined in all samples, especially the odd-MIF. Moreover, the inverse

relationship ($r^2 = 0.45$, $p < 0.01$) between $\Delta^{199}Hg$ and $\delta^{202}Hg$ was inconsistent with the

experimental results of photoreduction that generally showed positive correlation for the residual

510   Hg pool (here particles) (Bergquist and Blum, 2007; Zheng and Hintelmann, 2009). All these

arguments suggest that these processes may not be the major mechanism to produce large even

contrasting Hg isotope variation in Hg-enriched fine atmospheric particles. A recent study

reported Hg, isotopic fractionation during Hg^0 oxidation showed a positive relationship between

Δ^{199}Hg and δ^{202}Hg for Cl-initiated oxidation but a negative relationship for Br-initiated oxidation.

515   Though our PM$_{2.5}$ samples displayed also a decrease of Δ^{199}Hg with δ^{202}Hg (Fig. 2), similar to the Br-initiated oxidation, they had a Δ^{199}Hg/Δ^{201}Hg ratio (1.1) lower than that (1.6 ±0.3) of Br-initiated oxidation, and much lower than that (1.9 ± 0.2) of Cl-initiated oxidation (Sun et al., 2016). Though we cannot exclude the contribution of Hg^0 oxidation to PM$_{2.5}$-Hg, given the fact that halogen-initiated oxidation would not largely occur in in-land atmosphere boundary layer,

520   oxidation would not be a dominated controlling factor causing the seasonal variation of Hg isotopes in PM$_{2.5}$ particles. We thus suggest that the contributions from different sources may be the better scenario to explain the seasonal variation of Hg isotopic compositions we measured for the PM$_{2.5}$ samples.

5   Conclusions

525   In summary, our study reported, for the first time, large range and seasonal variations of both MDF and MIF of Hg isotopes in haze particulate (PM$_{2.5}$) samples collected from Beijing. The strong anthropogenic input to PM$_{2.5}$-Hg was evidenced by the high enrichment of Hg (and other "anthropophile" elements) and Hg isotopic compositions. Our data showed that mixing of variable contributing sources likely triggered the seasonal variation of Hg isotopic ratio. Major

530   potential contributing sources were identified by coupling Hg isotope data with other geochemical parameters (e.g. PM$_{2.5}$, EC, element concentrations) and meteorological data, and showed variable contribution in four seasons, with continuous industrial input (e.g. smelting, cement production and coal combustion) over the year and predominant contributions from coal combustion and biomass burning in winter and autumn, respectively. In addition to the local

535   and/or regional emissions, long-range transported Hg was probably also a contributor to PM$_{2.5}$-Hg, accounting for the relatively higher odd-MIF particularly found in spring and early summer. This study demonstrated the potential use of isotopes for tracing the sources of heavy metals and

their vectors in the atmosphere, and stressed the importance of studying toxic metals such as Hg

(and other heavy metals) in atmospheric particles while accessing the potential threat of hazes on

540   human health.

References

550   Bergquist, B. A., and Blum, J. D.: Mass-dependent and -independent fractionation of Hg isotopes
        by photoreduction in aquatic systems, Science, 318, 417-420, 2007.

Biswas, A., Blum, J. D., Bergquist, B. A., Keeler, G. J., and Xie, Z. Q.: Natural mercury isotope
        variation in coal deposits and organic soils, Environ. Sci. Technol., 42, 8303-8309, 2008.

Blum, J. D., and Bergquist, B. A.: Reporting of variations in the natural isotopic composition of
555   mercury, Anal. Bioanal. Chem., 388, 353-359, 2007.

Blum, J. D., Sherman, L. S., and Johnson, M. W.: Mercury isotopes in earth and environmental
        sciences, Annual Review of Earth and Planetary Sciences, 42, 249-269, 2014.

Buchachenko, A. L.: Mercury isotope effects in the environmental chemistry and biochemistry of
        mercury-containing compounds, Russian Chemical Reviews, 78, 319-328, 2009.

560   Cai, H., and Chen, J.: Mass-independent fractionation of even mercury isotopes, Science Bulletin,
        61, 116-124, 10.1007/s11434-015-0968-8, 2016.

Carignan, J., Estrade, N., Sonke, J. E., and Donard, O. F. X.: Odd isotope deficits in atmospheric
        Hg measured in Lichens, Environ. Sci. Technol., 43, 5660-5664, doi: 10.1021/Es900578v,
        2009.

565   Chen, J. B., Hintelmann, H., and Dimock, B.: Chromatographic pre-concentration of Hg from dilute aqueous solutions for isotopic measurement by MC-ICP-MS, J. Anal. At. Spectrom., 25, 1402-1409, 2010.

Chen, J. B., Hintelmann, H., Feng, X. B., and Dimock, B.: Unusual fractionation of both odd and even mercury isotopes in precipitation from Peterborough, ON, Canada, Geochim. Cosmochim.

570   Acta, 90, 33-46, 2012.

Chen, J. B., Gaillardet, J., Bouchez, J., Louvat, P., and Wang, Y. N.: Anthropophile elements in river sediments: Overview from the Seine River, France, Geochem. Geophys. Geosyst., 15, 4526-4546, 2014.

Das, R., Wang, X., Khezri, B., Webster, R. D., Sikdar, P. K., and Datta, S.: Mercury isotopes of

575   atmospheric particle bound mercury for source apportionment study in urban Kolkata, India, Elementa: Science of the Anthropocene, 4, 000098, doi: 10.12952/journal.elementa.000098, 2016.

Demers, J. D., Blum, J. D., and Zak, D. R.: Mercury isotopes in a forested ecosystem: Implications for air-surface exchange dynamics and the global mercury cycle, Global

580   Biogeochem. Cycles, 27, 222-238, 2013.

Demers, J. D., Sherman, L. S., Blum, J. D., Marsik, F. J., and Dvonch, J. T.: Coupling atmospheric mercury isotope ratios and meteorology to identify sources of mercury impacting a coastal urban‐industrial region near Pensacola, Florida, USA, Global Biogeochem Cy, 29, 1689-1705, 2015a.

585   Demers, J. D., Sherman, L. S., Blum, J. D., Marsik, F. J., and Dvonch, J. T.: Coupling atmospheric mercury isotope ratios and meteorology to identify sources of mercury impacting a coastal urban-industrial region near Pensacola, Florida, USA, Global Biogeochem. Cycles, 29, 1689-1705, 10.1002/2015GB005146, 2015b.

Eiler, J. M., Bergquist, B., Bourg, I., Cartigny, P., Farquhar, J., Gagnon, A., Guo, W., Halevy, I.,

590   Hofmann, A., Larson, T. E., Levin, N., Schauble, E. A., and Stolper, D.: Frontiers of stable isotope geoscience, Chem. Geol., 372, 119-143, http://dx.doi.org/10.1016/j.chemgeo.2014.02.006, 2014.

Enrico, M., Roux, G. L., Marusczak, N., Heimbürger, L.-E., Claustres, A., Fu, X., Sun, R., and Sonke, J. E.: Atmospheric Mercury Transfer to Peat Bogs Dominated by Gaseous Elemental

595   Mercury Dry Deposition, Environ. Sci. Technol., 50, 2405-2412, 10.1021/acs.est.5b06058, 2016.

Estrade, N., Carignan, J., and Donard, O. F. X.: Tracing and quantifying anthropogenic mercury sources in soils of northern France using isotopic signatures, Environ. Sci. Technol., 45, 1235-1242, 2011.

600   Feng, X. B., Foucher, D., Hintelmann, H., Yan, H. Y., He, T. R., and Qiu, G. L.: Tracing mercury contamination sources in sediments using mercury isotope compositions, Environ. Sci. Technol., 44, 3363-3368, 2010.

Fu, X., Marusczak, N., Wang, X., Gheusi, F., and Sonke, J. E.: Isotopic Composition of Gaseous Elemental Mercury in the Free Troposphere of the Pic du Midi Observatory, France, Environ.

605   Sci. Technol., 50, 5641-5650, 10.1021/acs.est.6b00033, 2016.

Fu, X. W., Feng, X. B., Zhu, W. Z., Zheng, W., Wang, S. F., and Lu, J. Y.: Total particulate and reactive gaseous mercury in ambient air on the eastern slope of the Mt. Gongga area, China, Appl. Geochem., 23, 408-418, 2008.

Fu, X. W., Feng, X. B., Qiu, G. L., Shang, L. H., and Zhang, H.: Speciated atmospheric mercury

610   and its potential source in Guiyang, China, Atmos. Environ., 45, 4205-4212, 2011.

Fu, X. W., Feng, X. B., Sommar, J., and Wang, S. F.: A review of studies on atmospheric mercury in China, Sci. Total Environ., 421, 73-81, doi: 10.1016/j.scitotenv.2011.09.089, 2012.

Fu, X. W., Heimburger, L. E., and Sonke, J. E.: Collection of atmospheric gaseous mercury for stable isotope analysis using iodine- and chlorine-impregnated activated carbon traps, J. Anal.

615   At. Spectrom., 29, 841-852, 2014.

Gao, J., Tian, H., Cheng, K., Lu, L., Zheng, M., Wang, S., Hao, J., Wang, K., Hua, S., Zhu, C., and Wang, Y.: The variation of chemical characteristics of PM2.5 and PM10 and formation causes during two haze pollution events in urban Beijing, China, Atmos. Environ., 107, 1-8, doi: 10.1016/j.atmosenv.2015.02.022, 2015.

620   Gao, Y., Nelson, E. D., Field, M. P., Ding, Q., Li, H., Sherrell, R. M., Gigliotti, C. L., Van Ry, D. A., Glenn, T. R., and Eisenreich, S. J.: Characterization of atmospheric trace elements on PM2.5 particulate matter over the New York–New Jersey harbor estuary, Atmos. Environ., 36, 1077-1086, http://dx.doi.org/10.1016/S1352-2310(01)00381-8, 2002.

Ghosh, S., Schauble, E. A., Lacrampe Couloume, G., Blum, J. D., and Bergquist, B. A.:

625   Estimation of nuclear volume dependent fractionation of mercury isotopes in equilibrium

liquid–vapor evaporation experiments, Chem. Geol., 336, 5-12, http://dx.doi.org/10.1016/j.chemgeo.2012.01.008, 2013.

Gratz, L. E., Keeler, G. J., Blum, J. D., and Sherman, L. S.: Isotopic composition and fractionation of mercury in Great Lakes precipitation and ambient air, Environ. Sci. Technol., 44, 7764-7770, 2010.

Han, L., Cheng, S., Zhuang, G., Ning, H., Wang, H., Wei, W., and Zhao, X.: The changes and long-range transport of PM2.5 in Beijing in the past decade, Atmos. Environ., 110, 186-195, doi: 10.1016/j.atmosenv.2015.03.013, 2015.

Hintelmann, H., and Lu, S. Y.: High precision isotope ratio measurements of mercury isotopes in cinnabar ores using multi-collector inductively coupled plasma mass spectrometry, Analyst, 128, 635-639, 2003.

Hintelmann, H., and Zheng, W.: Tracking geochemical transformations and transport of mercury through isotope fractionation, in: Environmental Chemistry and Toxicology of Mercury, John Wiley & Sons New York, 293-327, 2012.

Huang, M. J., Wang, W., Leung, H. M., Chan, C. Y., Liu, W. K., Wong, M. H., and Cheung, K. C.: Mercury levels in road dust and household TSP/PM2.5 related to concentrations in hair in Guangzhou, China, Ecotoxicol. Environ. Saf., 81, 27-35, 2012.

Huang, Q., Liu, Y. L., Chen, J. B., Feng, X. B., Huang, W. L., Yuan, S. L., Cai, H. M., and Fu, X. W.: An improved dual-stage protocol to pre-concentrate mercury from airborne particles for precise isotopic measurement, J. Anal. At. Spectrom., 30, 957-966, 2015.

Huang, R.-J., Zhang, Y., Bozzetti, C., Ho, K.-F., Cao, J.-J., Han, Y., Daellenbach, K. R., Slowik, J. G., Platt, S. M., and Canonaco, F.: High secondary aerosol contribution to particulate pollution during haze events in China, Nature, 514, 218-222, 2014.

Jackson, T. A., Muir, D. C. G., and Vincent, W. F.: Historical variations in the stable isotope composition of mercury in Arctic lake sediments, Environ. Sci. Technol., 38, 2813-2821, 2004.

Jackson, T. A., Whittle, D. M., Evans, M. S., and Muir, D. C. G.: Evidence for mass-independent and mass-dependent fractionation of the stable isotopes of mercury by natural processes in aquatic ecosystems, Appl. Geochem., 23, 547-571, 2008.

Jackson, T. A., Telmer, K. H., and Muir, D. C. G.: Mass-dependent and mass-independent variations in the isotope composition of mercury in cores from lakes polluted by a smelter:

Effects of smelter emissions, natural processes, and their interactions, Chem. Geol., 352, 27-46, 2013.

Jackson, T. A.: Evidence for mass-independent fractionation of mercury isotopes by microbial activities linked to geographically and temporally varying climatic conditions in Arctic and subarctic Lakes, Geomicrobiol. J., 32, 799-826, 2015.

Jiskra, M., Wiederhold, J. G., Bourdon, B., and Kretzschmar, R.: Solution speciation controls mercury isotope fractionation of Hg(II) sorption to goethite, Environ. Sci. Technol., 46, 6654-6662, 2012.

Jiskra, M., Wiederhold, J. G., Skyllberg, U., Kronberg, R.-M., Hajdas, I., and Kretzschmar, R.: Mercury Deposition and Re-emission Pathways in Boreal Forest Soils Investigated with Hg Isotope Signatures, Environ. Sci. Technol., 49, 7188-7196, 10.1021/acs.est.5b00742, 2015.

Kim, P. R., Han, Y. J., Holsen, T. M., and Yi, S. M.: Atmospheric particulate mercury: Concentrations and size distributions, Atmos. Environ., 61, 94-102, 2012.

Kim, S. H., Han, Y. J., Holsen, T. M., and Yi, S. M.: Characteristics of atmospheric speciated mercury concentrations (TGM, Hg(II) and Hg(p)) in Seoul, Korea, Atmos. Environ., 43, 3267-3274, 2009.

Li, J., Sommar, J., Wangberg, I., Lindqvist, O., and Wei, S. Q.: Short-time variation of mercury speciation in the urban of Goteborg during GOTE-2005, Atmos. Environ., 42, 8382-8388, 2008.

Lin, C. Y., Wang, Z., Chen, W. N., Chang, S. Y., Chou, C. C. K., Sugimoto, N., and Zhao, X.: Long-range transport of Asian dust and air pollutants to Taiwan: Observed evidence and model simulation, Atmos. Chem. Phys., 7, 423-434, doi: 10.5194/acp-7-423-2007, 2007.

Lin, H., Yuan, D., Lu, B., Huang, S., Sun, L., Zhang, F., and Gao, Y.: Isotopic composition analysis of dissolved mercury in seawater with purge and trap preconcentration and a modified Hg introduction device for MC-ICP-MS, J. Anal. At. Spectrom., 30, 353-359, doi: 10.1039/C4JA00242C, 2015a.

Lin, Y.-C., Hsu, S.-C., Chou, C. C. K., Zhang, R., Wu, Y., Kao, S.-J., Luo, L., Huang, C.-H., Lin, S.-H., and Huang, Y.-T.: Wintertime haze deterioration in Beijing by industrial pollution deduced from trace metal fingerprints and enhanced health risk by heavy metals, Environ. Pollut., doi: 10.1016/j.envpol.2015.07.044, 2015b.

Liu, B., Keeler, G. J., Dvonch, J. T., Barres, J. A., Lynam, M. M., Marsik, F. J., and Morgan, J. T.: Temporal variability of mercury speciation in urban air, Atmos. Environ., 41, 1911-1923, 2007.

Ma, J., Hintelmann, H., Kirk, J. L., and Muir, D. C. G.: Mercury concentrations and mercury isotope composition in lake sediment cores from the vicinity of a metal smelting facility in Flin Flon, Manitoba, Chem. Geol., 336, 96-102, 2013.

Malinovsky, D., Latruwe, K., Moens, L., and Vanhaecke, F.: Experimental study of mass-independence of Hg isotope fractionation during photodecomposition of dissolved methylmercury, J. Anal. At. Spectrom., 25, 950-956, 2010.

Masbou, J., Point, D., Sonke, J. E., Frappart, F., Perrot, V., Amouroux, D., Richard, P., and Becker, P. R.: Hg stable isotope time trend in ringed seals registers decreasing sea ice cover in the Alaskan Arctic, Environ. Sci. Technol., 49, 8977-8985, 2015.

Mbengue, S., Alleman, L. Y., and Flament, P.: Size-distributed metallic elements in submicronic and ultrafine atmospheric particles from urban and industrial areas in northern France, Atmos. Res., 135, 35-47, 10.1016/j.atmosres.2013.08.010, 2014.

Nzihou, A., and Stanmore, B.: The fate of heavy metals during combustion and gasification of contaminated biomass: A brief review, J. Hazard. Mater., 256–257, 56-66, doi: 10.1016/j.jhazmat.2013.02.050, 2013.

Rolison, J. M., Landing, W. M., Luke, W., Cohen, M., and Salters, V. J. M.: Isotopic composition of species-specific atmospheric Hg in a coastal environment, Chem. Geol., 336, 37-49, 2013.

Rudnick, R., and Gao, S.: Composition of the continental crust, Treatise on Geochemistry, 3, 1-64, 2003.

Saleh, R., Robinson, E. S., Tkacik, D. S., Ahern, A. T., Liu, S., Aiken, A. C., Sullivan, R. C., Presto, A. A., Dubey, M. K., Yokelson, R. J., Donahue, N. M., and Robinson, A. L.: Brownness of organics in aerosols from biomass burning linked to their black carbon content, Nature Geosci., 7, 647-650, doi: 10.1038/ngeo2220, 2014.

Schauble, E. A.: Role of nuclear volume in driving equilibrium stable isotope fractionation of mercury, thallium, and other very heavy elements, Geochim. Cosmochim. Acta, 71, 2170-2189, 2007.

715   Schleicher, N. J., Schäfer, J., Blanc, G., Chen, Y., Chai, F., Cen, K., and Norra, S.: Atmospheric particulate mercury in the megacity Beijing: Spatio-temporal variations and source apportionment, Atmos. Environ., 109, 251-261, doi: 10.1016/j.atmosenv.2015.03.018, 2015.

Seigneur, C., Abeck, H., Chia, G., Reinhard, M., Bloom, N. S., Prestbo, E., and Saxena, P.: Mercury adsorption to elemental carbon (soot) particles and atmospheric particulate matter,

720   Atmos. Environ., 32, 2649-2657, 1998.

Selin, N. E.: Global biogeochemical cycling of mercury: A review, Annu. Rev. Env. Resour., 34, 43-63, 2009.

Sherman, L. S., Blum, J. D., Johnson, K. P., Keeler, G. J., Barres, J. A., and Douglas, T. A.: Mass-independent fractionation of mercury isotopes in Arctic snow driven by sunlight, Nature

725   Geosci., 3, 173-177, 2010.

Sherman, L. S., Blum, J. D., Keeler, G. J., Demers, J. D., and Dvonch, J. T.: Investigation of local mercury deposition from a coal-fired power plant using mercury isotopes, Environ. Sci. Technol., 46, 382-390, 2012.

Sherman, L. S., Blum, J. D., Franzblau, A., and Basu, N.: New insight into biomarkers of human

730   mercury exposure using naturally occurring mercury stable isotopes, Environ. Sci. Technol., 47, 3403-3409, 2013.

Sherman, L. S., Blum, J. D., Dvonch, J. T., Gratz, L. E., and Landis, M. S.: The use of Pb, Sr, and Hg isotopes in Great Lakes precipitation as a tool for pollution source attribution, Sci. Total Environ., 502, 362-374, doi: 10.1016/j.scitotenv.2014.09.034, 2015.

735   Smith, C. N., Kesler, S. E., Blum, J. D., and Rytuba, J. J.: Isotope geochemistry of mercury in source rocks, mineral deposits and spring deposits of the California coast ranges, USA, Earth. Planet. Sci. Lett., 269, 398-406, 2008.

Smith, R. S., Wiederhold, J. G., and Kretzschmar, R.: Mercury isotope fractionation during precipitation of metacinnabar (β-HgS) and montroydite (HgO), Environ. Sci. Technol., 49,

740   4325-4334, doi: 10.1021/acs.est.5b00409, 2015.

Song, S., Wu, Y., Jiang, J., Yang, L., Cheng, Y., and Hao, J.: Chemical characteristics of size-resolved PM2.5 at a roadside environment in Beijing, China, Environ. Pollut., 161, 215-221, doi: 10.1016/j.envpol.2011.10.014, 2012.

Song, Y., Tang, X. Y., Xie, S. D., Zhang, Y. H., Wei, Y. J., Zhang, M. S., Zeng, L. M., and Lu, S.

745   H.: Source apportionment of PM2.5 in Beijing in 2004, J. Hazard. Mater., 146, 124-130, 2007.

Sonke, J. E.: A global model of mass independent mercury stable isotope fractionation, Geochim. Cosmochim. Acta, 75, 4577-4590, 2011.

Streets, D. G., Hao, J., Wu, Y., Jiang, J., Chan, M., Tian, H., and Feng, X.: Anthropogenic mercury emissions in China, Atmos. Environ., 39, 7789-7806, doi: 10.1016/j.atmosenv.2005.08.029, 2005.

Sun, G., Sommar, J., Feng, X., Lin, C.-J., Ge, M., Wang, W., Yin, R., Fu, X., and Shang, L.: Mass-Dependent and -Independent Fractionation of Mercury Isotope during Gas-Phase Oxidation of Elemental Mercury Vapor by Atomic Cl and Br, Environ. Sci. Technol., 50, 9232-9241, 10.1021/acs.est.6b01668, 2016.

Sun, R., Sonke, J. E., Heimbürger, L.-E., Belkin, H. E., Liu, G., Shome, D., Cukrowska, E., Liousse, C., Pokrovsky, O. S., and Streets, D. G.: Mercury stable isotope signatures of world coal deposits and historical coal combustion emissions, Environ. Sci. Technol., 48, 7660-7668, doi: 10.1021/es501208a, 2014.

Sun, R. Y., Heimburger, L. E., Sonke, J. E., Liu, G. J., Amouroux, D., and Berail, S.: Mercury stable isotope fractionation in six utility boilers of two large coal-fired power plants, Chem. Geol., 336, 103-111, 2013.

Waheed, A., Li, X. L., Tan, M. G., Bao, L. M., Liu, J. F., Zhang, Y. X., Zhang, G. L., and Li, Y.: Size Distribution and Sources of Trace Metals in Ultrafine/Fine/Coarse Airborne Particles in the Atmosphere of Shanghai, Aerosol Sci. Technol., 45, 163-171, 2011.

Wang, H., Kawamura, K., and Shooter, D.: Carbonaceous and ionic components in wintertime atmospheric aerosols from two New Zealand cities: Implications for solid fuel combustion, Atmos. Environ., 39, 5865-5875, 2005.

Wang, L., Liu, Z., Sun, Y., Ji, D., and Wang, Y.: Long-range transport and regional sources of PM 2.5 in Beijing based on long-term observations from 2005 to 2010, Atmos. Res., 157, 37-48, 2015a.

Wang, Z., Chen, J., Feng, X., Hintelmann, H., Yuan, S., Cai, H., Huang, Q., Wang, S., and Wang, F.: Mass-dependent and mass-independent fractionation of mercury isotopes in precipitation from Guiyang, SW China, C. R. Geosci., 347, 358-367, doi: 10.1016/j.crte.2015.02.006, 2015b.

Wang, Z. W., Zhang, X. S., Chen, Z. S., and Zhang, Y.: Mercury concentrations in size-fractionated airborne particles at urban and suburban sites in Beijing, China, Atmos. Environ., 40, 2194-2201, 2006.

Wiederhold, J. G., Cramer, C. J., Daniel, K., Infante, I., Bourdon, B., and Kretzschmar, R.: Equilibrium mercury isotope fractionation between dissolved Hg(II) species and thiol-bound Hg, Environ. Sci. Technol., 44, 4191-4197, 2010.

780 Won, J. H., Park, J. Y., and Lee, T. G.: Mercury emissions from automobiles using gasoline, diesel, and LPG, Atmos. Environ., 41, 7547-7552, 2007.

Xiu, G. L., Cai, J., Zhang, W. Y., Zhang, D. N., Bueler, A., Lee, S. C., Shen, Y., Xu, L. H., Huang, X. J., and Zhang, P.: Speciated mercury in size-fractionated particles in Shanghai ambient air, Atmos. Environ., 43, 3145-3154, 2009.

785 Xu, L. L., Chen, J. S., Niu, Z. C., Yin, L. Q., and Chen, Y. T.: Characterization of mercury in atmospheric particulate matter in the southeast coastal cities of China, Atmos. Pollut. Res., 4, 454-461, 2013.

Xu, M., Yan, R., Zheng, C., Qiao, Y., Han, J., and Sheng, C.: Status of trace element emission in a coal combustion process: A review, Fuel Process. Technol., 85, 215-237, doi: 790 10.1016/S0378-3820(03)00174-7, 2004.

Yin, R., Feng, X., and Shi, W.: Application of the stable-isotope system to the study of sources and fate of Hg in the environment: A review, Appl. Geochem., 25, 1467-1477, http://dx.doi.org/10.1016/j.apgeochem.2010.07.007, 2010.

Yin, R. S., Feng, X. B., and Meng, B.: Stable mercury isotope variation in rice plants (Oryza 795 sativa L.) from the Wanshan mercury mining district, SW China, Environ. Sci. Technol., 47, 2238-2245, 2013.

Yin, R. S., Feng, X. B., and Chen, J. B.: Mercury stable isotopic compositions in coals from major coal producing fields in China and their geochemical and environmental implications, Environ. Sci. Technol., 48, 5565-5574, doi: 10.1021/Es500322n, 2014.

800 Yuan, S., Zhang, Y., Chen, J., Kang, S., Zhang, J., Feng, X., Cai, H., Wang, Z., Wang, Z., and Huang, Q.: Large variation of mercury isotope composition during a single precipitation event at Lhasa city, Tibetan Plateau, China, Procedia Earth and Planetary Science, 13, 282-286, 2015.

Zambardi, T., Sonke, J. E., Toutain, J. P., Sortino, F., and Shinohara, H.: Mercury emissions and stable isotopic compositions at Vulcano Island (Italy), Earth. Planet. Sci. Lett., 277, 236-243, 805 2009.

Zhang, H., Yin, R. S., Feng, X. B., Sommar, J., Anderson, C. W. N., Sapkota, A., Fu, X. W., and Larssen, T.: Atmospheric mercury inputs in montane soils increase with elevation: Evidence from mercury isotope signatures, Sci. Rep., 3, 2013a.

Zhang, L., Wang, S. X., Wang, L., and Hao, J. M.: Atmospheric mercury concentration and chemical speciation at a rural site in Beijing, China: Implications of mercury emission sources, Atmos. Chem. Phys., 13, 10505-10516, 2013b.

Zhang, L., Wang, S. X., Wang, L., Wu, Y., Duan, L., Wu, Q. R., Wang, F. Y., Yang, M., Yang, H., Hao, J. M., and Liu, X.: Updated emission inventories for speciated atmospheric mercury from anthropogenic sources in China, Environ. Sci. Technol., 49, 3185-3194, 2015.

Zhang, Y., Schauer, J. J., Zhang, Y., Zeng, L., Wei, Y., Liu, Y., and Shao, M.: Characteristics of particulate carbon emissions from real-world Chinese coal combustion, Environ. Sci. Technol., 42, 5068-5073, doi: 10.1021/es7022576, 2008.

Zheng, M., Salmon, L. G., Schauer, J. J., Zeng, L., Kiang, C. S., Zhang, Y., and Cass, G. R.: Seasonal trends in PM2.5 source contributions in Beijing, China, Atmos. Environ., 39, 3967-3976, doi: 10.1016/j.atmosenv.2005.03.036, 2005a.

Zheng, W., Foucher, D., and Hintelmann, H.: Mercury isotope fractionation during volatilization of Hg(0) from solution into the gas phase, J. Anal. At. Spectrom., 22, 1097-1104, 2007.

Zheng, W., and Hintelmann, H.: Mercury isotope fractionation during photoreduction in natural water is controlled by its Hg/DOC ratio, Geochim. Cosmochim. Acta, 73, 6704-6715, 2009.

Zheng, W., and Hintelmann, H.: Isotope fractionation of mercury during its photochemical reduction by low-molecular-weight organic compounds, J. Phys. Chem. A, 114, 4246-4253, 2010a.

Zheng, W., and Hintelmann, H.: Nuclear field shift effect in isotope fractionation of mercury during abiotic reduction in the absence of light, J. Phys. Chem. A, 114, 4238-4245, 2010b.

Zheng, X., Liu, X., Zhao, F., Duan, F., Yu, T., and H, C.: Seasonal characteristics of biomass burning contribution to Beijing aerosol, Sci. China Ser. B, 48, 481-488, doi: 10.1360/042005-15, 2005b.

Zhou, J., Zhang, R., Cao, J., Chow, J. C., and Watson, J. G.: Carbonaceous and ionic components of atmospheric fine particles in Beijing and their impact on atmospheric visibility, Aerosol Air Qual. Res., 12, 492-502, 2012.

Zhu, J., Wang, T., Talbot, R., Mao, H., Yang, X., Fu, C., Sun, J., Zhuang, B., Li, S., Han, Y., and Xie, M.: Characteristics of atmospheric mercury deposition and size-fractionated particulate mercury in urban Nanjing, China, Atmos. Chem. Phys., 14, 2233-2244, 2014.

840 **Figure 1.** Seasonal variations of $PM_{2.5}$ (a) and elemental carbon (b) contents, Hg concentrations (c) and Hg isotopic ratios (d-f) of the $PM_{2.5}$ samples. For each box plot, the median is the 50th percentile and error bars extend from 75th percentile to the maximum value (upper) and from the 25th percentile to the minimum value (lower). The tiny square in each box represents the seasonal mean value.
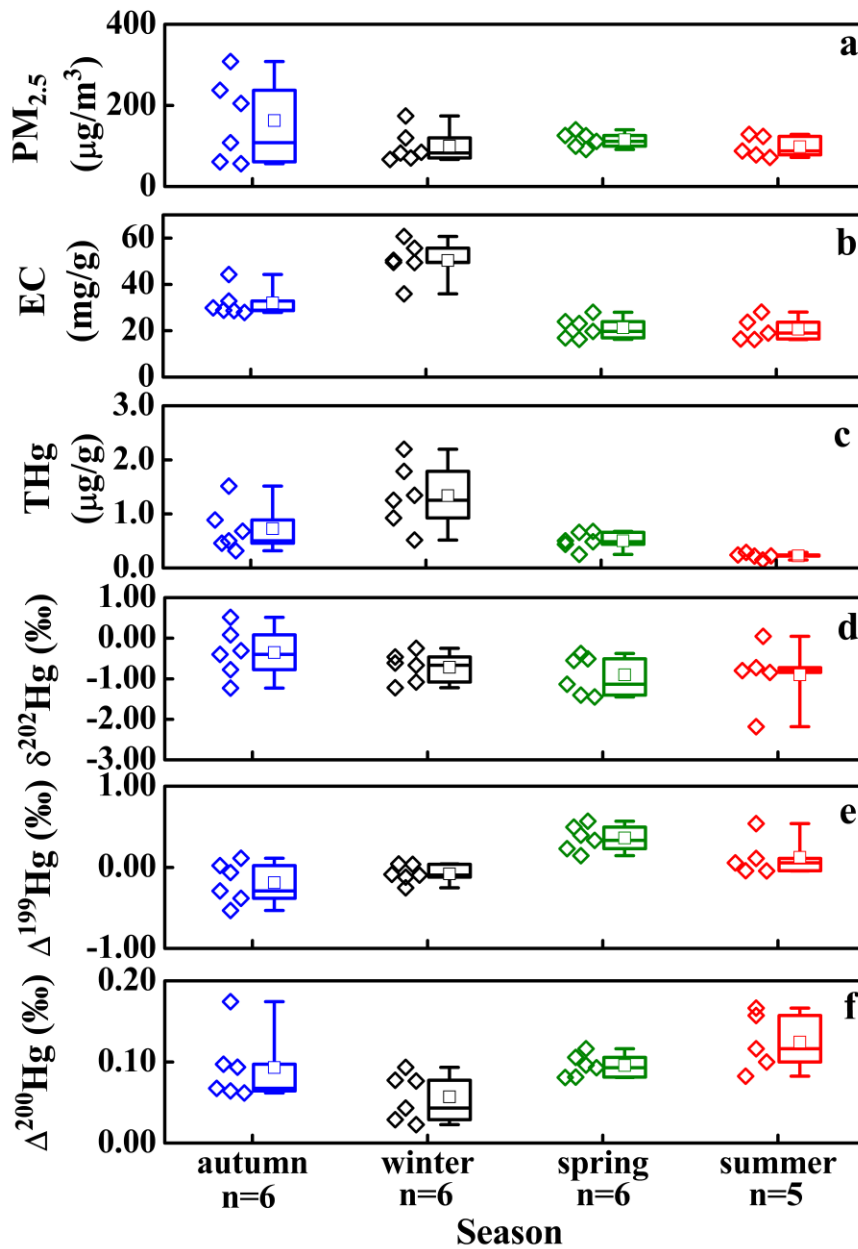
845

Figure 2. Shown are relationships between Δ^{199}Hg and δ^{202}Hg (a) and Δ^{201}Hg (b) for 23 PM$_{2.5}$

samples. The gray areas are the ranges of Hg isotope compositions of potential source materials.
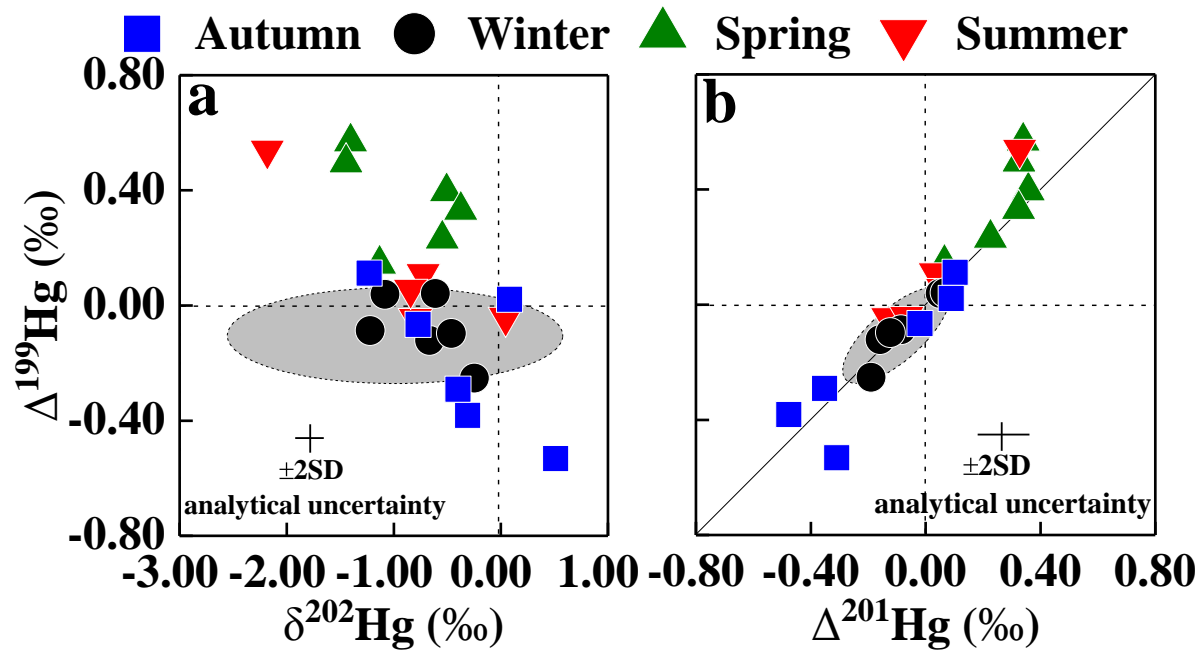
Figure 3. Comparison of isotopic compositions between the selected potential source materials and the PM$_{2.5}$ samples. The δ^{202}Hg values of PM$_{2.5}$-Hg are within the ranges of the source materials, but the Δ^{199}Hg values are out of the range, suggesting contribution from other unknown sources or MIF during atmospheric processes.
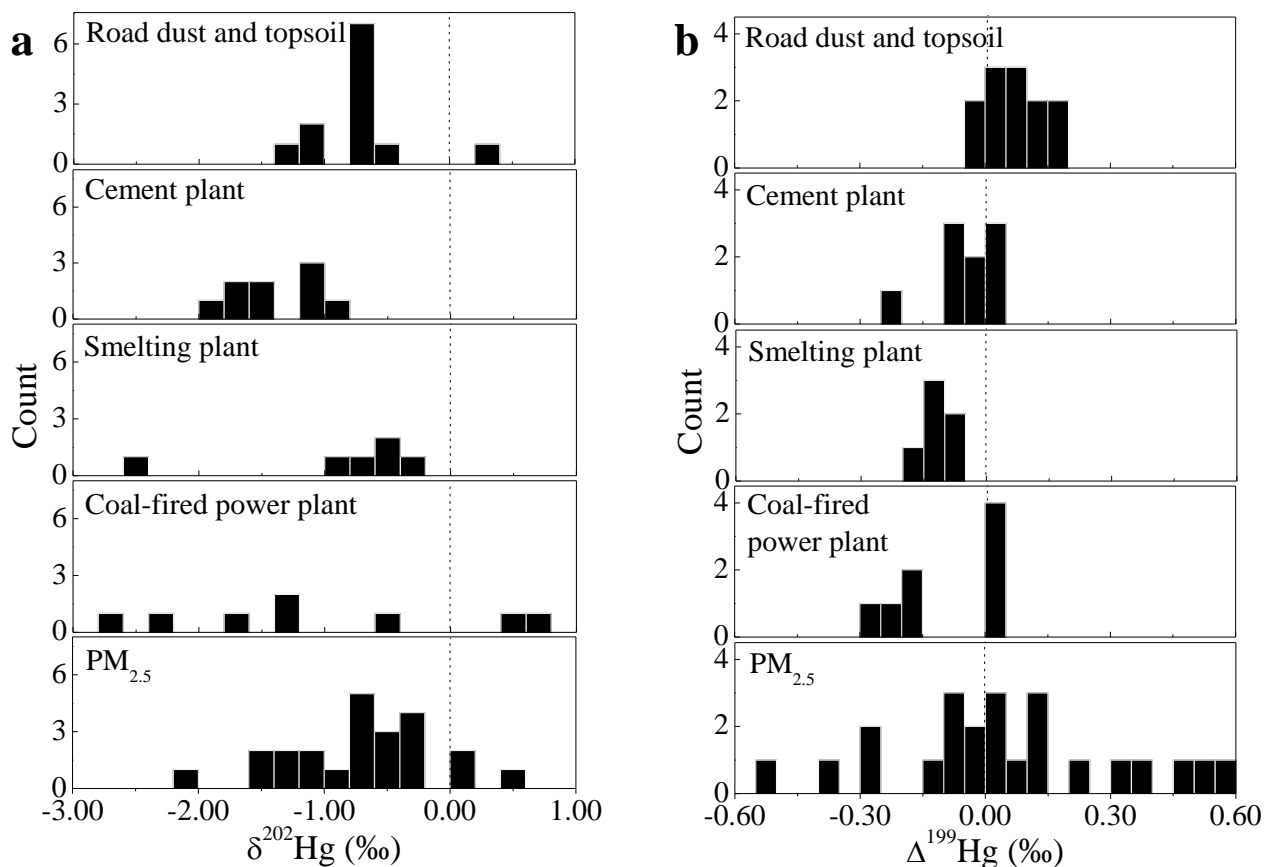
Figure 4. Plots of the volumetric Hg concentration versus PM$_{2.5}$ content (a), EC content (b), and concentrations of Co (c) and Zn (d) for the PM$_{2.5}$ samples. In both (c) and (d), only 14 PM$_{2.5}$ samples were showed with Co and Zn datasets, as 9 other PM$_{2.5}$ samples were used up during isotope and OC/EC analyses.
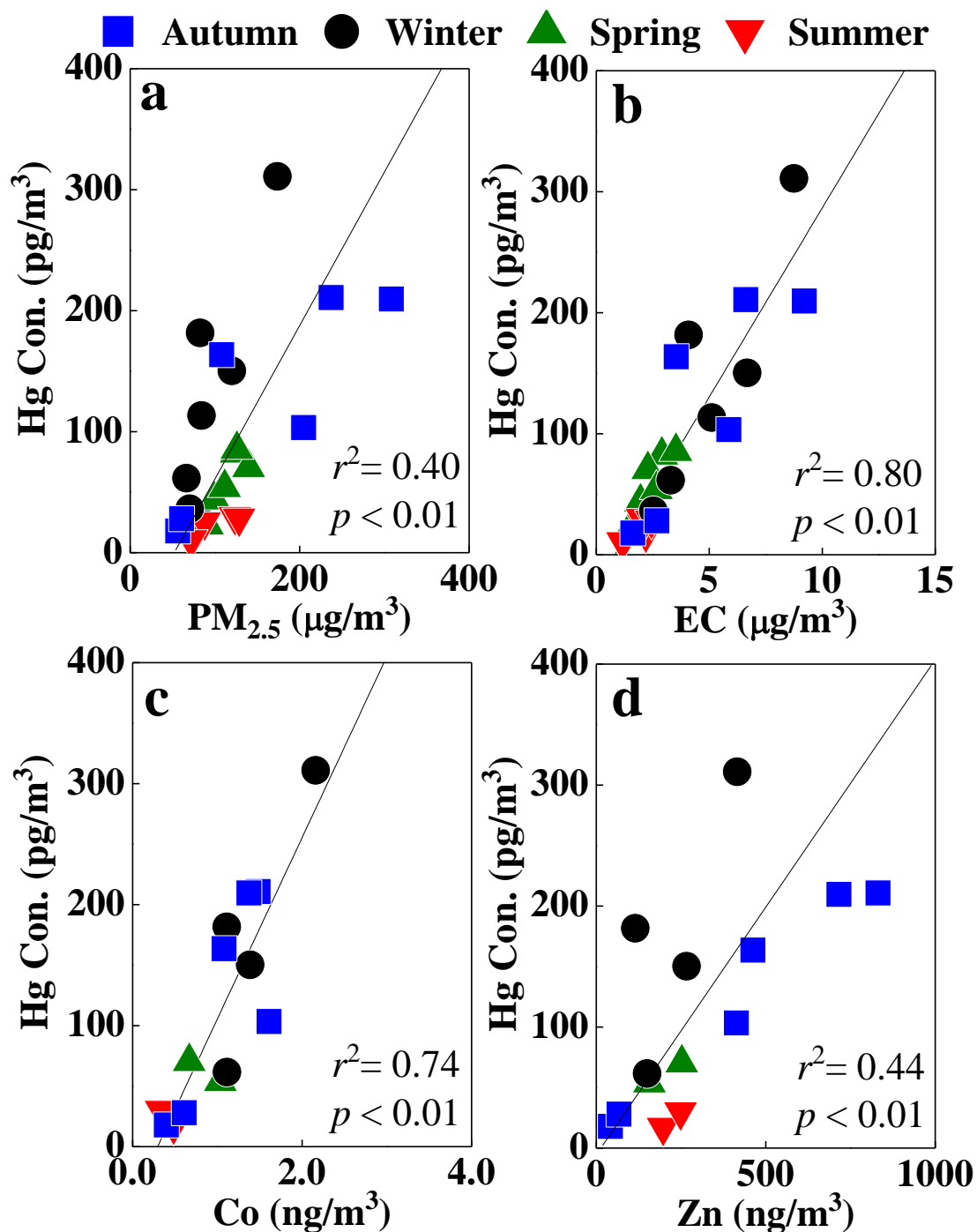
Figure 5. Correlations between Hg isotopic composition (δ^{202}Hg and Δ^{199}Hg) and Co/Al (a and b)

and EC/Al (c and d) elemental mass ratios. In all cases, δ^{202}Hg values are positively correlated to, and Δ^{199}Hg values are negatively correlated to the Co/Al and EC/Al ratios.
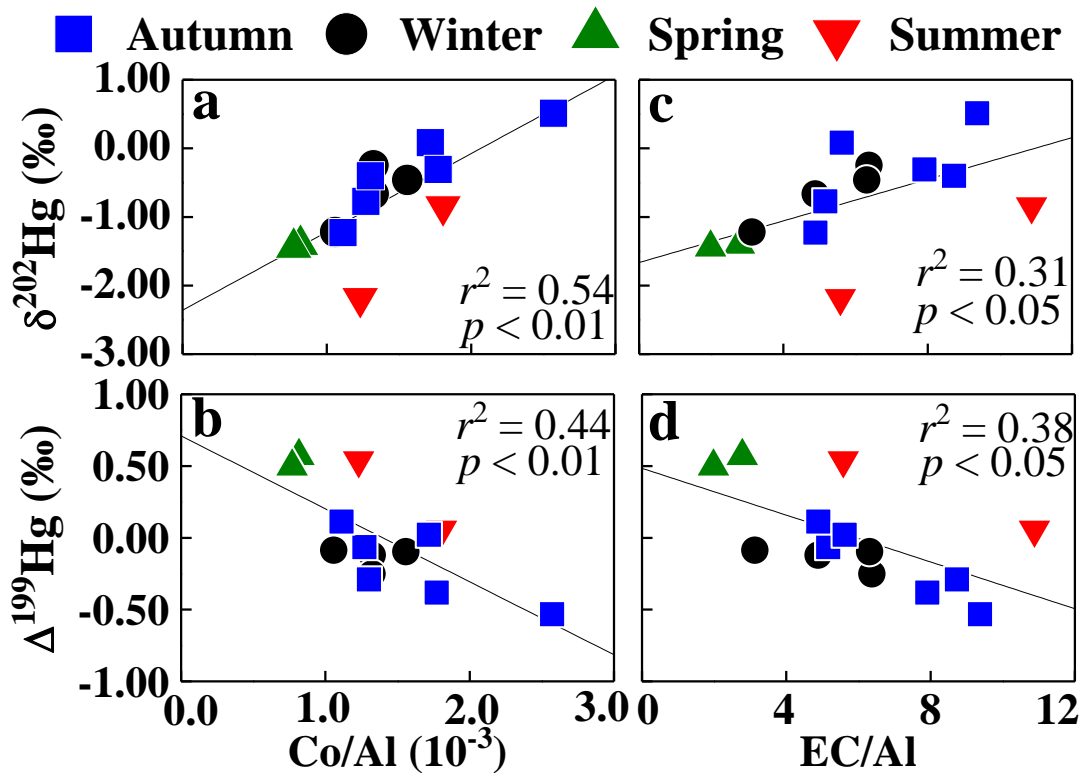
Figure 6. Correlations between Hg isotopic composition (δ^{202}Hg and Δ^{199}Hg) and Hg enrichment factor EF(Hg) (a and b). δ^{202}Hg value is positively correlated to the EF(Hg), while Δ^{199}Hg value is negatively correlated to the EF(Hg).
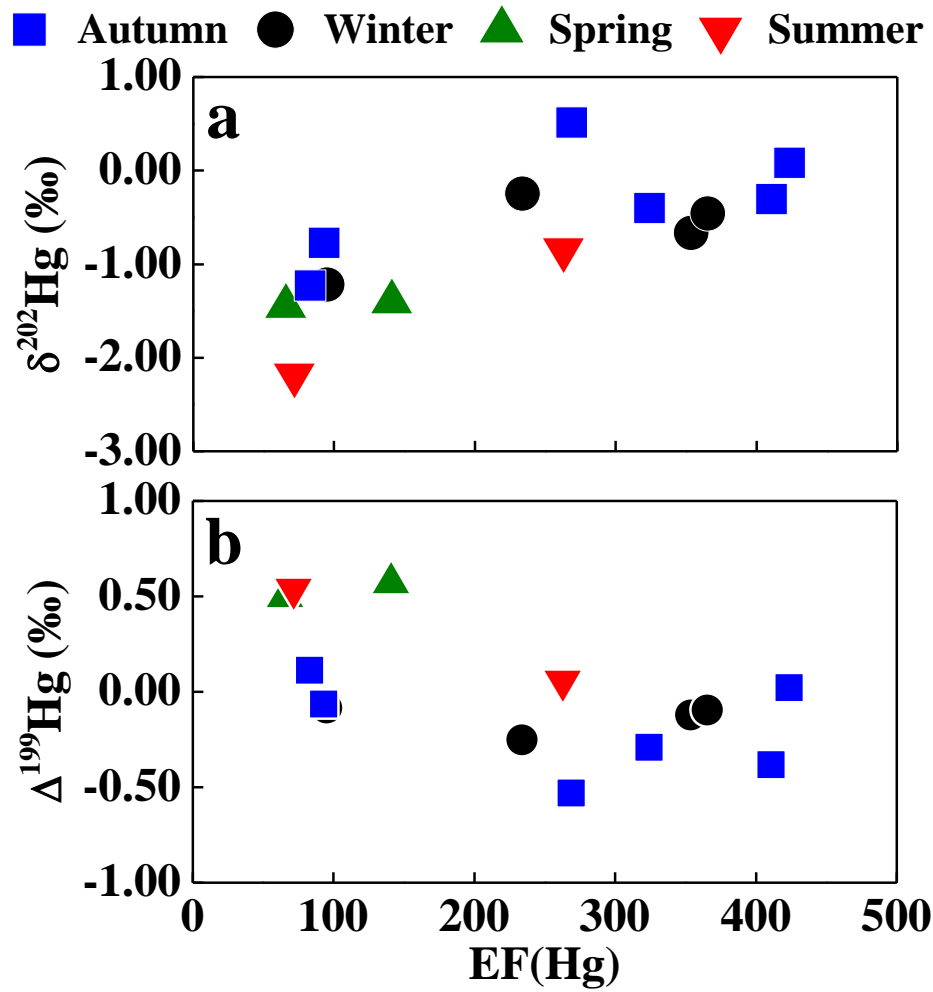
Figure 7. Correlations between Zn/Al ratios and EC contents suggest seasonal characteristics of PM$_{2.5}$ sources with seasonally unique Δ^{199}Hg signatures (in ‰).